A SUCCESSFUL USE OF l_{max} AS AN UPPER LIMIT FOR NUCLEAR FUSION CHANNEL

G. S. Hassan

Physics Department, Assiut University,
71516 Assiut, Egypt
E-mail: galalsh@yahoo.com

ABSTRACT

To calculate the complete fusion cross section over partial waves, as a function of the excitation energy, the maximum value of angular momentum l_{max} represents the upper limit of that summation. An effective definition for that limit has been checked. Also a comparison with the fusion and critical limits, l_{fus} and l_{cr} respectively, has been displayed. The effects of the nuclear part, of the barrier height and the approximation technique have been checked to approach the best fit of the measured fusion excitation functions.

***Keywords*:** Barrier, Channel, Critical limit, Iteration, Attractive force
PACS: 25.88; 25.70Gh; 25.70Jj

INTRODUCTION

The nuclear fusion is a low density phenomenon and several calculations have been made to search for the nuclear structure effects and enhancement in fusion cross sections at sub-barrier energies. The complete fusion mechanism in the heavy ion collisions strongly depends on the entrance channel peculiarities: mass (charge) asymmetry, shell structure of interacting nuclei, beam energy, angular momentum and impact parameter [1]. Recent experimental measurements of nuclear reaction cross sections show a systematic suppression of the complete fusion cross section for both weakly bound and tightly bound nuclei, at energies above the Coulomb barrier such as the partial capture of the projectile (incomplete fusion), whereas the elastic breakup mode is found to play a minor role [2,3].

Significant results could be found by concerning the effect of the nuclear part of the barrier. The proximity potential provides a simple recipe for the variation of the nuclear potential with the sizes of the collision partners [1,4]. The Bass potential: has been based on the liquid-drop model and general geometrical arguments to give the nucleus-nucleus potential for spherical nuclei and frozen densities [5]. The Woods-Saxon potential presents the real part of the optical model potential taking into account that above the fusion barrier, the imaginary part of that potential has been neglected [6].The Unified potential has been obtained by generalizing the modified nuclear surface energy

due to the liquid drop model and is given in terms of a double volume integral of a Yukawa – plus-exponential folding function [7].

The fusion excitation functions will be discussed in terms of the limiting angular momentum for fusion l_{fus}. This angular momentum is determined by the properties of both the entrance channel and the compound nucleus. In principle, the transmission probability from the entrance channel into the compound nucleus will occur only if the initial conditions are favorable and if appropriate states are available in the compound nucleus. If however one of these conditions is satisfied trivially in a specific situation, then the other one will become the limiting factor for compound nucleus formation.

METHODS OF CALCULATION

Due to barrier penetration models (BPM), the reaction cross section is given by partial wave summation over a definite channel of energy E as:

$$\sigma_{rec} = \pi\lambda^2 \sum_{\ell=0}^{\infty} (2\ell+1) T_\ell(E) P_\ell(E) \qquad (1)$$

where λ, T_l(E) and P_l(E) are the asymptotic wave length, the transmission coefficient and the probability of a specific process, respectively [8]. For fusion $\sigma_{rec} = \sigma_{fus}$ the higher limit of the summation becomes $l_{max,}$ which has been defined here, as that value of *l*-over which the summation (1) adds negligible terms [3]. Three terms represent the barrier height, namely the Coulomb, and nuclear components as:

$$V_B(R_{fus}) = V_C(R_{fus}) + V_l(R_{fus}), \qquad (2)$$

with the third part is the *l*-dependent centrifugal or the rotational energy at the top of the barrier [9]: $V_l(r) = \hbar^2 l(l+1)/(2\mu r^2)$.

Hence, the total barrier becomes $V(r,l) = V_B(r) + V_l(r)$.

For any entrance channel energy E, l_{max} determines the two conditions:

$$E = V(R_{fus}, l_{max}) \quad \text{and} \quad dV(R_{fus}, l_{max})/dr = 0$$

From which we get:

$$l_{max} = (-1 + (1 - 4S_E)^{1/2})/2 \qquad (3)$$

So that

$$S_E = 2\pi (R_{fus})^3 \{[(1 - (d/dr)] V_B(R_{fus}) - E_{cm}\}/\{\hbar^2 (R_{fus}+2)\}$$

Thus, Eq. (1) becomes: $$\sigma_{fus} = \pi\lambda^2 \sum_{l=0}^{l_{max}} (2l+1) T_l \qquad (4)$$

A smooth cut-off for fusion using the more realistic treatment of WKB approximation evaluates T_l(E): $T_l = 1/\{1+\exp[2\pi(V-E_{cm})/(\hbar\omega)]\}$,

where $\mu = \left\{\left(d^2V(r,l)/dr^2\right)/\right\}^{1/2}_{R_{fus}, l_{max}}$, whereas, eplacing summation by integration gives a sharp cutoff formula:

$$\sigma_{fus}(E) = (\hbar\mu R^2/2E)\ln(1+\exp\{(2\pi/\hbar\mu)(E - V_B(r))\}) \qquad (1b)$$

In a sharp cut-off approximation [10], the simplest treatment gives:

$$T_l = 1 \quad \text{for} \quad l \le l_{max}$$
$$= 0 \quad \text{for} \quad l > l_{max}$$

with the corresponding excitation function for fusion as:

$$\sigma_{fus}(E_{cm}) = \sigma_G(1 - V_B(R_{fus})/E_{cm}), \qquad (5)$$

where σ_G is the geometrical cross section at the barrier, and R_{fus} is the barrier radius.

For l greater than l_{max} the real potential no longer has a pocket, and it has been expressed as an l- cutoff or l_{cr} for complete fusion above which the centrifugal potential is so large that it prevents attractive fusion between the two colliding nuclei, and the fusion cross-section drops strongly. Also l_{cr} has been defined as the specific angular momentum at which the partial level width for fission is equal to that for evaporation, for which l_{cr} could be calculated [11] from:

$$\sigma_{fus} = (\hbar^2/2E_{cm})(l_{cr}+1)^2 \qquad (6)$$

RESULTS AND DISCUSSION

Table (1) lists the barrier height and radius for some pairs in comparison with those given by analytical formulations of the ion-ion interaction potential (AFIP and DPFB) [1], displaying the effect of the nuclear potential model on the results and giving good agreements with both of them. Table (2) displays l_{max} values calculated by Eq. (3) and those given by iteration as a value at which the summation (4) adds negligible terms [3]. We can notice that l_{max} values given by Eq. (3) are larger than l_{cr} values, especially for light pairs which indicates the effects of the enhancements of coupled channels on the measured cross sections while those given by iteration are smaller, this could be interpreted due to a wide range of enhancements of coupled channels at higher energies. Table (3) lists l_{max}, calculated using either unified or proximity potentials for the undertaken pairs used to fit the excitation functions concerning the more new measured data. Also, we tried to choose the most effective potential models recovering all measured data, using both of sharp and smooth cut-off approximations at the same radius (R_{fus}).

Table 1. Barrier heights (V_P, V_U and V_W calculated using the proximity, unified and Woods-Saxon potential, respectively) and R_{fus} [7], in comparison with those calculated by Arora [1], (1 for (AFIP) and 2 for (DPFB), respectively)

Pojectile	Target	R_{fus}	V_b	R_{b1}	V_{b1}	R_{b2}	V_{b2}
^{16}O	^{16}O	8.10	10.72P	8.20	10.61	8.07	10.94
^{16}O	^{20}Ne	8.29	13.15P	8.35	13.05	8.23	13.22
^{16}O	^{24}Mg	8.46	15.52P	8.52	15.38	8.38	15.42
^{16}O	^{26}Mg	8.58	15.30P	8.62	15.18	8.45	15.20
^{16}O	^{28}Si	8.60	17.83P	8.67	17.65	8.51	17.56
^{18}O	^{28}Si	8.76	17.2PU	8.80	17.34	8.63	17.24
^{16}O	^{40}Ca	8.97	24.1PU	9.07	24.03	8.89	23.71
^{18}O	^{24}Mg	8.61	15.23P	8.65	15.11	8.48	15.13
^{20}Ne	^{20}Ne	8.47	16.14P	8.50	15.98	8.41	16.00

^{20}Ne	^{40}Ca	9.12	29.29U	9.17	29.55	9.14	28.93
^{24}Mg	^{24}Mg	8.78	22.1PU	8.80	22.21	8.77	21.90
^{24}Mg	^{26}Mg	8.90	21.8PU	8.95	21.92	8.86	21.60
^{24}Mg	^{32}S	9.03	28.33U	9.02	28.74	9.10	28.08
^{24}Mg	^{28}Si	8.91	25.08U	8.94	25.51	8.94	25.02
^{26}Mg	^{32}S	9.15	27.98U	9.17	28.38	9.19	27.71
^{24}Mg	^{34}S	9.13	28.04U	9.21	28.41	9.17	27.77
^{26}Mg	^{34}S	9.24	28.1PU	9.31	28.06	9.26	27.41
^{28}Si	^{28}Si	9.04	28.9PW	9.04	29.33	9.12	28.63
^{28}Si	^{30}Si	9.14	28.85U	9.18	28.98	9.20	28.28
^{30}Si	^{30}Si	9.25	28.26U	9.32	28.65	9.28	27.94
^{32}S	^{40}Ca	9.47	45.27U	9.52	45.37	9.69	44.06
^{40}Ca	^{40}Ca	9.66	54.05P	9.78	55.10	9.90	53.86

Table 2. l_{max1} calculated by Eq. (3) up to the E_{cm} range, and l_{max2} by iteration from Eq. (5) in comparison with l_{cr} deduced from Eq. (6).

Pojectile	Target	l_{max1}	E_{cm}	l_{max2}	l_{cr}
^{16}O	^{16}O	27.38	34.1	22	24.98
^{16}O	^{20}Ne	32.23	41.15	24	29.85
^{16}O	^{24}Mg	36.79	48.55	27	34.46
^{16}O	^{26}Mg	37.87	47.9	27	35.48
^{16}O	^{28}Si	41.67	56.0	33	39.20
^{18}O	^{28}Si	41.25	54.75	30	37.39
^{16}O	^{40}Ca	53.50	76.55	46	51.47
^{18}O	^{24}Mg	37.11	47.85	31	33.33
^{20}Ne	^{20}Ne	38.72	50.62	31	36.20
^{20}Ne	^{40}Ca	65.16	94.95	57	63.49
^{24}Mg	^{24}Mg	51.38	70.4	42	49.13
^{24}Mg	^{26}Mg	53.07	69.65	43	50.72
^{24}Mg	^{32}S	64.63	91.5	56	62.73
^{24}Mg	^{28}Si	58.15	80.75	50	56.04
^{26}Mg	^{32}S	64.01	90.2	54	61.74
^{24}Mg	^{34}S	65.58	90.25	54	63.82
^{26}Mg	^{34}S	64.62	88.95	57	62.35
^{28}Si	^{28}Si	65.83	93.0	57	64.03
^{28}Si	^{30}Si	67.16	92.2	59	65.48
^{30}Si	^{30}Si	67.00	91.45	50	64.82
^{32}S	^{40}Ca	97.14	145.9	85	97.40
^{40}Ca	^{40}Ca	116.12	178.75	101	118.27

Table 3. For Figs. (1-8), the barrier radius and height R_{fus} (fm) and V_B (MeV) and the values l_{max} used to fit recently measured data

System	R_{fus} (fm)	V_B (MeV)	E_{cm} (MeV)	l_{max1}	Reference
^{6}Li + ^{28}Si	8.02	6.7	9 -20	15	12
^{4}He + ^{64}Zn	9.39	8.4	7.5 - 16	20	13
^{6}Li + ^{64}Ni	9.19	12.0	10 – 25.5	25	14
^{4}He +^{208}Pb	11.32	19.6	20 - 30	33	15
^{4}He +^{238}U	11.64	21.4	19.7 – 31.5	36	16
^{12}C + ^{89}Y	9.85	24.2	30 - 46	54	17

$^{11}B + ^{159}Tb$	10.96	39.6	35.8 - 60	76	18
$^{12}C + ^{159}Tb$	10.9	47.6	52 - 82	88	19
$^{12}C + ^{208}Pb$	11.37	57.7	52 - 88	100	20
$^{16}O + ^{176}Yb$	11.8	66.45	59 - 95	122	21
$^{19}F + ^{192}Os$	11.43	79.1	75 - 94	147	22
$^{20}Ne + ^{208}Pb$	11.54	93.7	85 - 107	166	23
$^{27}Al + ^{197}Au$	11.57	115.7	107 - 150	212	24

The results of our calculations are given in the form of graphs displaying the dependence of fusion cross-section on energy. For all the illustrated figures, the curves are numbered due to:
Curve (1) using unified nuclear force and WKB, Eq. (1) up to l_{max} from Eq. (3)
Curve (2) using unified nuclear force and the logarithmic form, Eq. (1a)
Curve (3) using proximity nuclear force and WKB, Eq. (1) up to l_{max} from Eq. (3)
Curve (4) using proximity nuclear force and the logarithmic form, Eq. (1a)

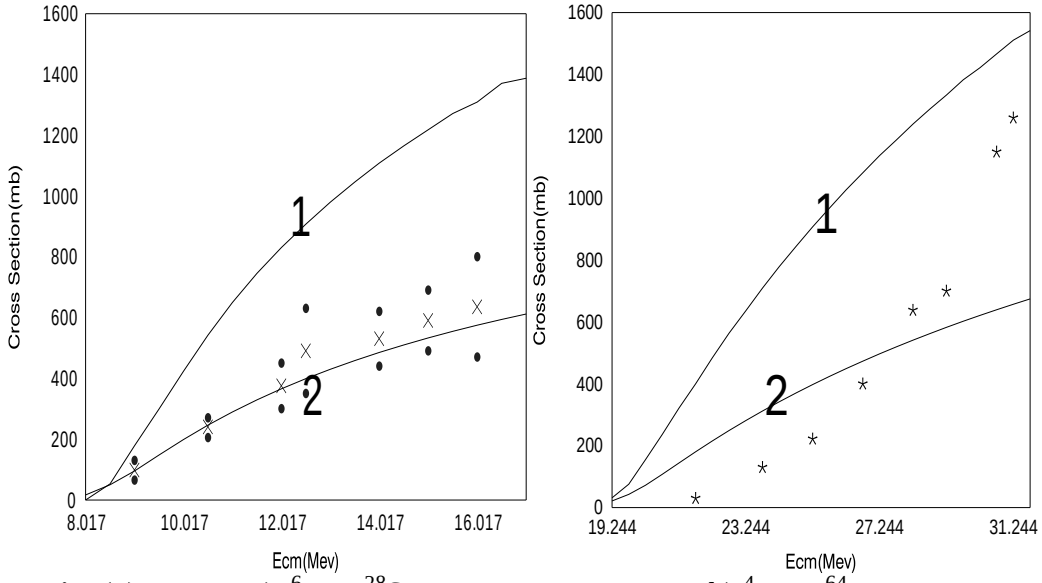

Fig. (1) a) $^{6}Li + ^{28}Si$ b) $^{4}He + ^{64}Zn$

Figure 1. Fusion excitation functions for: a) $^{6}Li + ^{28}Si$ and b) $^{4}He + ^{64}Zn$. The curve (1) is in good agreement with the measured data, from reference[12] for $^{6}Li + ^{28}Si$ while curve (2) is the more acceptable for $^{4}He + ^{64}Zn$ with the measured data, from reference[13].

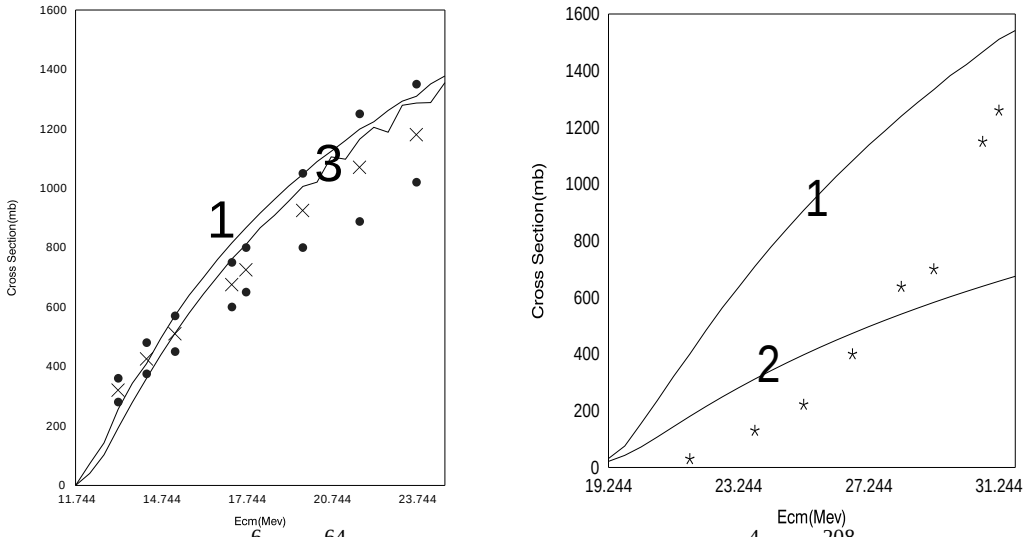

Fig. (2) a) $^{6}Li + {}^{64}Ni$ b) $^{4}He + {}^{208}Pb$

Figure 2. Fusion excitation functions for: a) $^{6}Li + {}^{64}Ni$ and b) $^{4}He + {}^{208}Pb$. The curves (1,3) are in good agreement with the measured data, from reference[14] for $^{6}Li + {}^{64}Ni$ while curve (2) is the more acceptable for $^{4}He + {}^{208}Pb$ with the measured data, from reference[15], in contrast to the acceptance for our l_{max} definition.

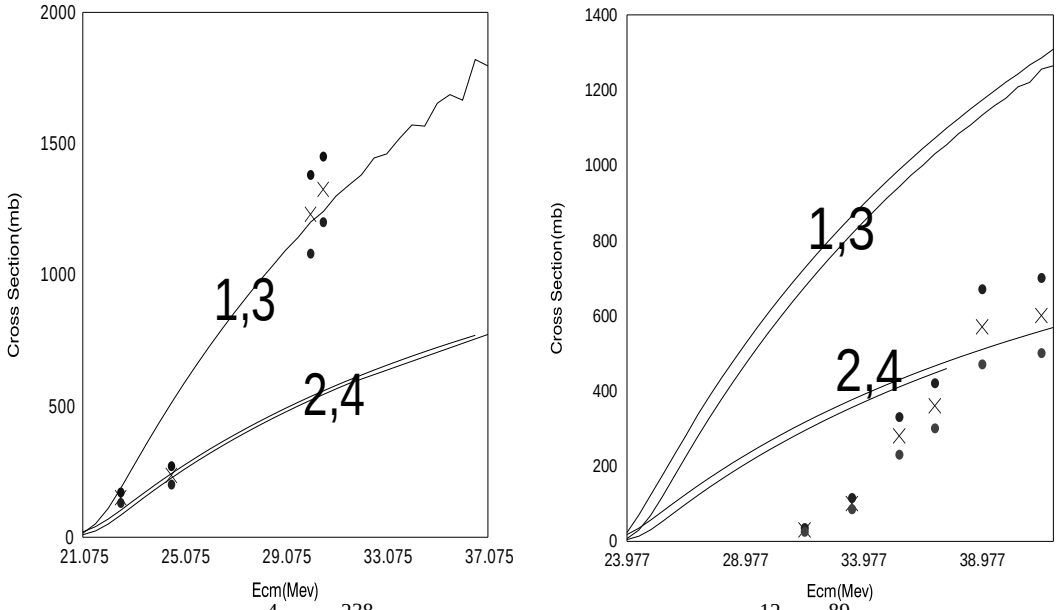

Fig. (3) a) $^{4}He + {}^{238}U$ b) $^{12}C + {}^{89}Y$

Figure 3. Fusion excitation functions for: a) $^{4}He + {}^{238}U$ and b) $^{12}C + {}^{89}Y$. The curves (1,3) are in good agreement with the most of the measured data, from reference[16] for $^{4}He + {}^{238}U$, while curves (2,4) are noticed in more acceptance for $^{12}C + {}^{89}Y$ with the measured data, from reference[17], in contrast to the acceptance for l_{max} definition

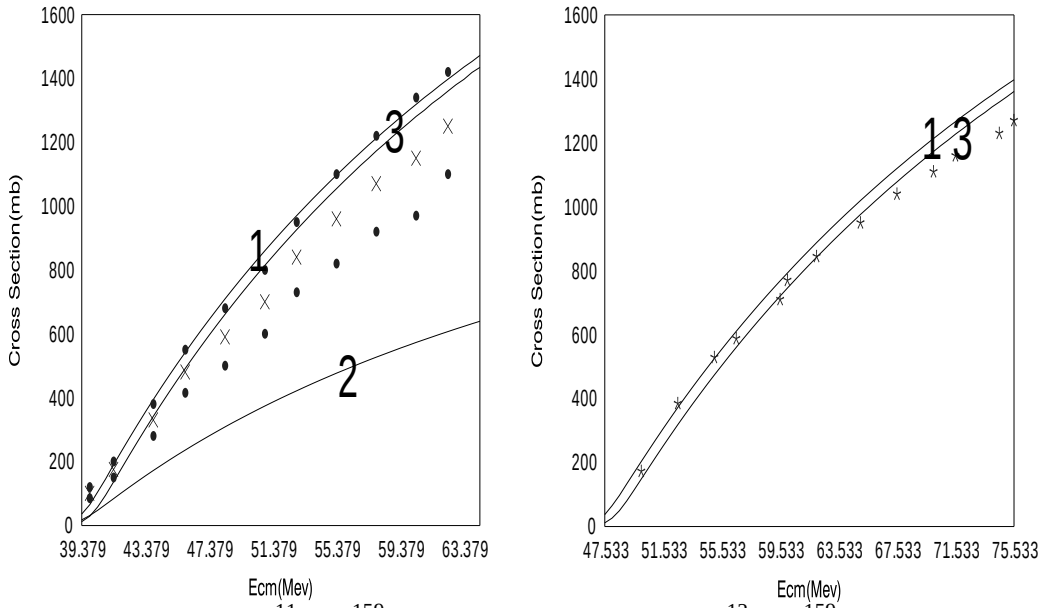

Fig. (4) a) $^{11}B + {}^{159}Tb$ b) $^{12}C + {}^{159}Tb$

Figure 4. Fusion excitation functions for: a) $^{11}B + {}^{159}Tb$ and b) $^{12}C + {}^{159}Tb$. The curves (1,3) give the best fit for the measured data, from reference[18] for $^{11}B + {}^{159}Tb$ as well as a high accurate fitting for $^{12}C + {}^{159}Tb$ with the measured data, from reference[19]. It is a clear view of the acceptance for l_{max} definition.

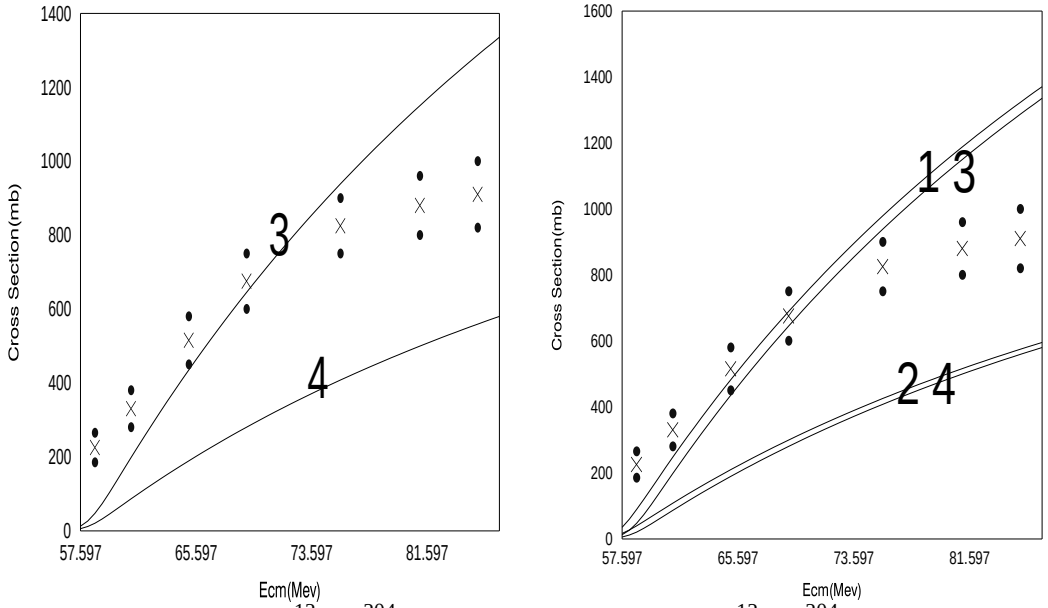

Fig. (5) a) $^{12}C + {}^{204}Pb$ b) $^{12}C + {}^{204}Pb$

Figure 5. Fusion excitation functions for: a,b) $^{12}C + {}^{204}Pb$. The curves(1,3) give the best fit for the measured data, from reference[20], while both of curves (2,4) failed to fit any of the measured data. Similarly the second figure clear that. This means that our choice for l_{max} definition seems to be in safe for wider energies as well as for wider range of fusing ions. The more interest note is that the effect of the excitation function calculation technique is more significant than that for choice of nuclear force formula.

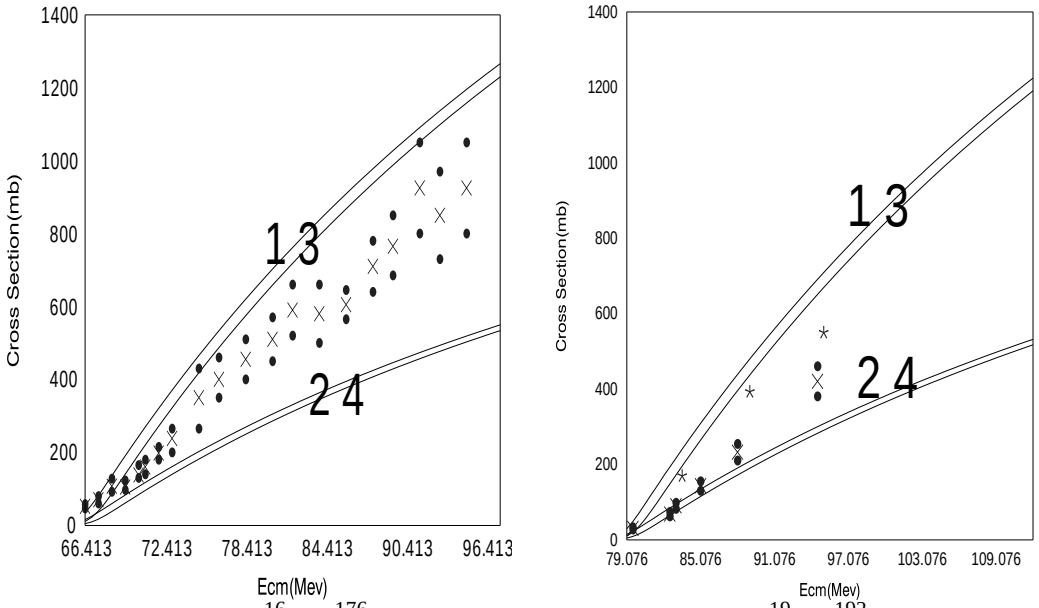

Fig. (6) a) $^{16}O + ^{176}Yb$ b) $^{19}F + ^{192}Os$

Figure 6. Fusion excitation functions for: a) $^{16}O + ^{176}Yb$, and b) $^{19}F + ^{192}Os$. The curves (1,3) give the more acceptable agreement with the measured data, from reference [21] for $^{16}O + ^{176}Yb$ as well as a high accurate fitting for $^{19}F + ^{192}Os$, especially at higher energies than above the barrier with the measured data, from reference [22]. It interprets a good acceptance for l_{max} definition.

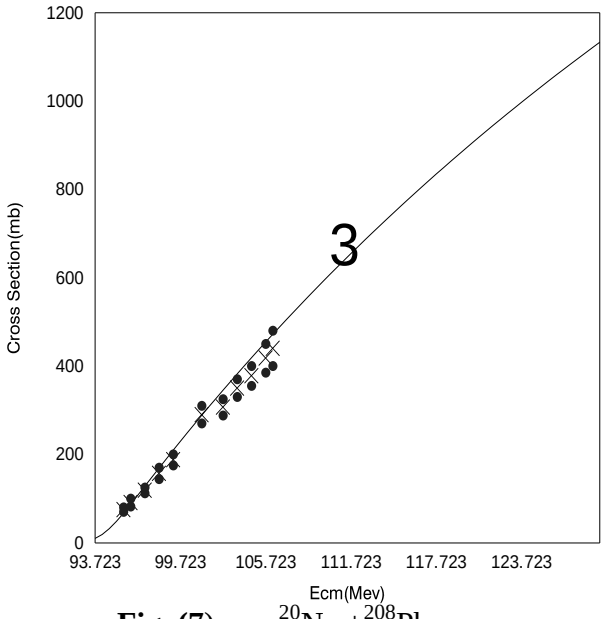

Fig. (7) $^{20}Ne + ^{208}Pb$

Figure 7. Fusion excitation functions for $^{20}Ne + ^{208}Pb$. The proximity potential together with the WKB approximation technique up to the value l_{max} as defined, Eq.(3), namely curves (3) gives successfully an exact fit of the new measured data, from reference [23] and introduces the clear proof.

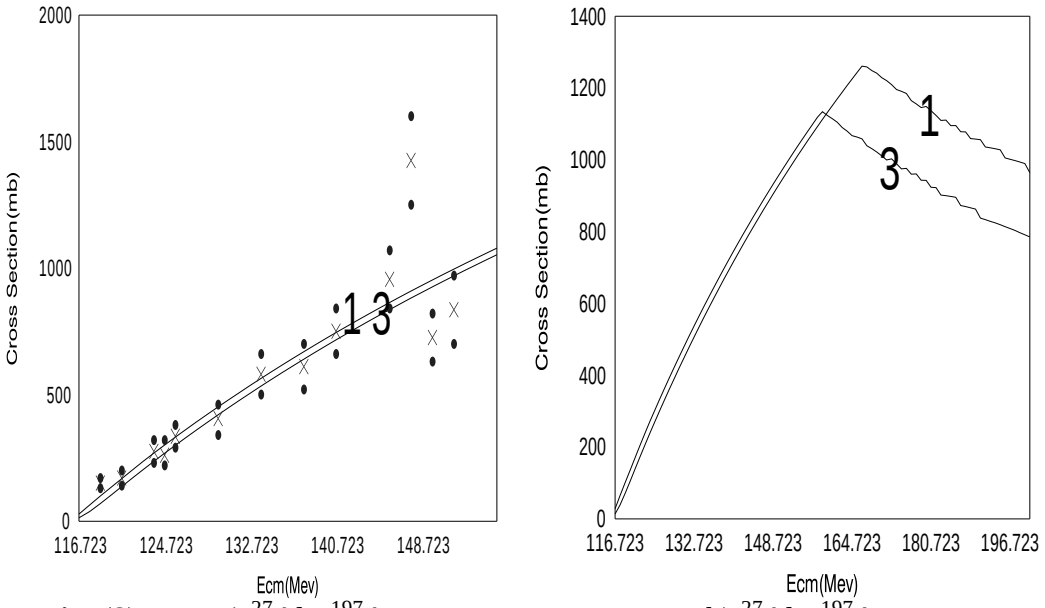

Fig. (8) a) $^{27}Al + ^{197}Au$ b) $^{27}Al + ^{197}Au$

Figure 8. Fusion excitation functions for: a,b) $^{27}Al + ^{197}Au$. Two more interest notes are clear, first is that curve (3) is the perfect for fitting of the new measured data, from reference [24] and second is that the measured data display a peak on the excitation function while the theoretical calculations due to both unified and proximity potentials and the WKB approximation technique up to the value l_{max} as defined by Eq.(3), namely curves (1,3) display similar peak but higher in energy as shown on b). This note will be interpreted during the forthcoming work.

The following comments may be given on the figures:

In Fig. (1), curve (1) is in good agreement with the measured data [12] for $^{6}Li + ^{28}Si$**,** while curve (2) is more acceptable for $^{4}He + ^{64}Zn$ with the measured data [13]. In Fig. (2), curves (1,3) are in good agreement with the measured data [14] for $^{6}Li + ^{64}Ni$**,** while curve (2) is more acceptable for $^{4}He + ^{208}Pb$ with the measured data [15]. In Fig. (3)**,** the curves (1,3) are in good agreement with the most of the measured data [16] for $^{4}He + ^{238}U$, while curves (2,4) gives more acceptance for $^{12}C + ^{89}Y$ with the measured data [17]. In Fig. (4), the curves (1,3) give the best fit for the measured data [18] for $^{11}B + ^{159}Tb$ as well as a high accurate fitting for $^{12}C + ^{159}Tb$ with the measured data [19]. In Fig. (5)**,** the curves (1,3) give the best fit for the measured data of [20]. It is of interest note is that the effect of the excitation function calculation technique is more significant than that for choice of nuclear force formula. In Fig. (6), the curves (1,3) display acceptable agreement with the measured data [21] for $^{16}O + ^{176}Yb$ as well as a high accurate fitting for $^{19}F + ^{192}Os$ with the measured data [22]. In Fig. (7), curve (3) gives successfully an exact fit of the new measured data [23]. In Fig. (8), curve (3) is the perfect for measured data [24] of $^{27}Al + ^{197}Au$ and measured data display a peak on the excitation function while the theoretical calculations, namely curves (1,3) display similar peak but higher in energy.

From the figures, it is clear that the unified potential is in agreement with most of the more recently measured data for light nuclei and extends to include different interacting pairs up to intermediate ions but it fails to fit the data with heavy nuclei. It

seems also accepted for both unified and proximity potential to fit data over wider excitation energy ranges. In few cases we found that the proximity potential is more applicable for light nuclei than for heavier ones

CONCLUSION

Tables (1-3) conclude that, for fusion excitation functions, the limiting angular momentum l_{max} given by Eq. (3), could be successfully used to display good agreement of the calculated and measured excitation functions, as well as good agreement with both l_{fus} values given by Bass model [6] and l_{cr} values, Eq. (6) and make a significant consideration to the enhancements of coupled channels, especially for higher excitation energies .Also we can note that l_{max} values are larger than both of those given by Eqs. (5,6) , especially for light pairs which indicates the effects of the enhancements of coupled channels on the measured cross sections while those given by iteration are smaller, this could be interpreted due to a wide range of enhancements of coupled channels at higher energies .

From figures, there is a harmony between unified potential and proximity potential when using WKB technique for excitation function calculations. This harmony could be attributed to the origin of models, since the unified potential stems from the independent particle model while the proximity comes from the liquid drop model. A nice note is that as measured data display a peak on the excitation function, the similar peak due to our calculations using both unified and proximity potentials and the WKB approximation technique up to the value l_{max} as defined by Eq. (3), namely curves (1,3) display similar peak but higher in energy as shown on b). This note is in contrast to the quantum tunneling phenomena and will be interpreted during the forthcoming work.

REFERENCES

[1] R. Arora et al, *Eur. Phys. J.* , **A8**, 103-114 (2000), A.K. Nasirov, 5th ASRC Int. Workshop, (JAEA), Tokai, Japan, March (2012)
[2] J. Lei and A.M. Moro, *Phys. Rev. Lett.*, Feb 1;122(4):042503 (2019)
[3] G.S. Hassan, *Bull. Russian Acad. Sci.*, (Physics), (2002)
[4] M. Dasgupta etal, *Ann. Rev. Nucl. Part. Sci.*, **48**, 401-61 (1998)
[5] W. Zippwe and H. Czakanski, *Z. Phys. A* **377**, 309 (1990).
[6] Y. Nagashima et al, *Phys. Rev. C* **33**, 176-184 (1986)
[7] H.J. Krappe et al, *Phys. Rev. C* **20**, 3, 992-1013 (1979).
and H.J. Krappe, A.J. Sierk, *Phys. Rev. C* **20**, 992 (1979).
[8] L.C. Vaz and J.M. Alexander, *Phys. Rep*. **69**, 5, (1981)
and G.S. Hassan et al, *Acta Phys. Pol. B* **31**, 1799-1809 (2000)
[9] A.K. Mohanty, et al, *Phys. Rev. C* **46**, 5, 2012-2018 (1992)
and R. Satchler and W.G. Love, *Phys. Lett. B* **65**, 415 (1976)
[10] T. Udagawa et al , *Phys. Rev. C* **32**, 1, 124-135 (1985)
[11] H. Kusawake et al, *Radiochemica Acta* **69**, 65-75 (1995)
[12] Mandira Sinha et al, *European Physical Journal A* **44**, 403 (2010)
[13] V. Scuderi et al, *Phys. Rev. C* **84**, 64604 (2011)
[14] Md. Moin Shaikh et al, *Phys. Rev. C* **91**, 34615 (2015)

[15] S.M. Lukyanov et al, *Phys. Lett. B* **670**, 321 (2009)
[16] R. Raabe et al, *Nature* **431**, 823 (2004)
[17] C.S.M. Palshetkar et al, *Phys. Rev. C* **82**, 044608 (2010)
[18] A. Mukherje et al, *Phys. Lett. B* **636**, 91 (2006)
[19] Abhishek Yadav et al, *Phys. Rev. C* **85**, 34614 (2012)
[20] R.N. Sagaidak et al, *Phys. Rev. C* **68**, 014603 (2003)
[21] Tapan Rajbongshi et al, *Phys. Rev. C* **93**, 54622 (2016)
[22] K. Mahata et al, *Nucl. Phys. A* **720**, 209 (2003)
[23] E. Piasecki et al, *Phys. Rev. C* **85**, 54608 (2012)
[24] Y.X. Watanabe et al, *European Physical Journal A* **10**, 373 (2001)